Supporting Information

Temperature Dependence Studies of New Particle Formation from Methanesulfonic Acid

and Amines/Ammonia

Haihan Chen and Barbara J. Finlayson-Pitts*

Department of Chemistry
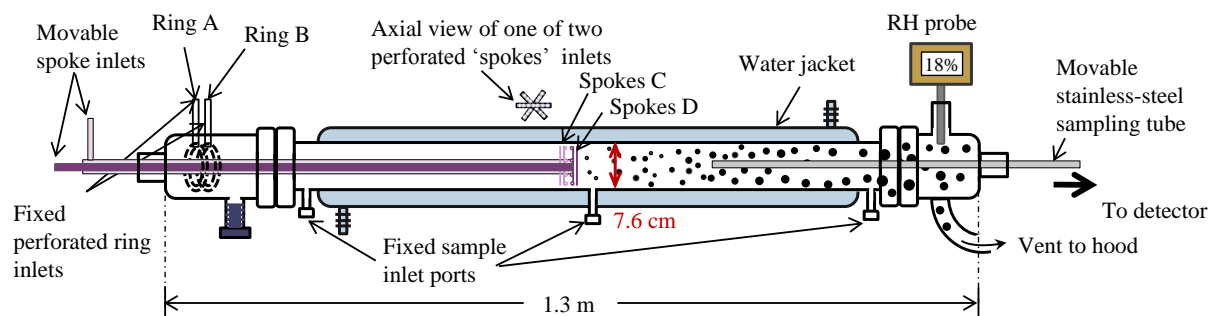University of California, Irvine
Irvine, CA 92697

Figure S1. Schematic of the flow reactor.

Description of the Flow Reactor

The main section of the flow reactor has a diameter of 7.6 cm and a length of 1.3 m, and is
water jacketed for temperature control. The flow reactor has two ring inlets (Fig. S1, ring A and
ring B) and two spoke inlets (Fig. S1, spokes C and spokes D), to easily change the mixing order
of gas phase precursors. A ¼" stainless steel movable sampling tube is mounted on the
downstream end-cap (Fig. S1) for sampling of particles and gaseous precursors from the radial
center of the flow reactor. The reaction time, controlled by adjusting the position of the
sampling tube while keeping the spoke inlets at a fixed position, was calculated using the
distance between the end of the sampling tube and spokes D, and a previously determined
conversion factor (0.14 s cm^{-1}). The spoke inlets were perforated in a way in order to rapidly
mix gas species from the upstream rings and the spokes and shorten the mixing length of the
flow reactor. As discussed in our previous paper, the turbulent flow around the spokes becomes

28 laminar 7-10 cm downstream corresponding to 1-1.5 s reaction time. The time travelled in the
29 sampling tube (1.9 s) was not included in the reaction time under the assumption that reactions
30 are quenched rapidly in the sampling tube due to wall uptake of any remaining MSA or base. A
31 purge air generator (Model 75-62; Parker Balston) was used to provide dry compressed air for
32 this study. The dry air was passed through carbon/alumina media (Perma Pure, LLC), and a 0.1
33 μm filter (DIF-N70; Headline Filters) for further purification.

The Effect of Temperature on Wall Losses of Gaseous Precursors and Particles

35 Diffusion of gas phase precursors decreases with decreasing temperature which in principle
36 would lower the wall losses, leaving higher concentrations in the gas phase to form more
37 particles; however, as shown in Table S1, diffusion coefficients of gaseous precursors are
38 relatively constant over the small temperature range covered in the current study. The change of
39 temperature also has an effect on the sink capacity of the walls for gases. If, as expected, rates of
40 desorption of adsorbed species back into the gas phase have a larger temperature dependence
41 than collision rates with the walls, the net wall losses will increase with decreasing temperature,
42 giving smaller gas phase concentrations which will lead to smaller particle formation rather than
43 larger, opposite to the experimental observations.

44 The effect of temperature on wall losses of particles was also examined by introducing pre-
45 formed particles into the flow reactor at different temperatures with or without water vapor.
46 Briefly, particles were pre-formed from MSA-MA by introducing flows of MSA (0.2 slpm),
47 dried purified air (3.6 slpm) and MA (0.2 slpm) from three separate inlets into a 5-L glass bulb.
48 The initial concentrations inside the glass bulb were 21.0×10^{10} cm^{-3} MSA and 19.8×10^{10} cm^{-3}
49 MA. The flow out of the glass bulb was passed through a denuder to remove residual gases, and
50 then introduced into the glass flow reactor from ring B. Additional purified air flows were
51 introduced from ring A (10 slpm), spokes C (2 slpm) and spokes D (1 slpm) to bring the total
52 flow to 17 slpm. Water vapor was added by passing the 10 slpm air flow through a water
53 bubbler prior to introduction into the flow reactor from ring A. Wall losses of particles were
54 examined by measuring particle size distributions as a function of time at varied temperatures
55 under both dry and humid conditions. As shown in Figure S2, the experiments indicate that
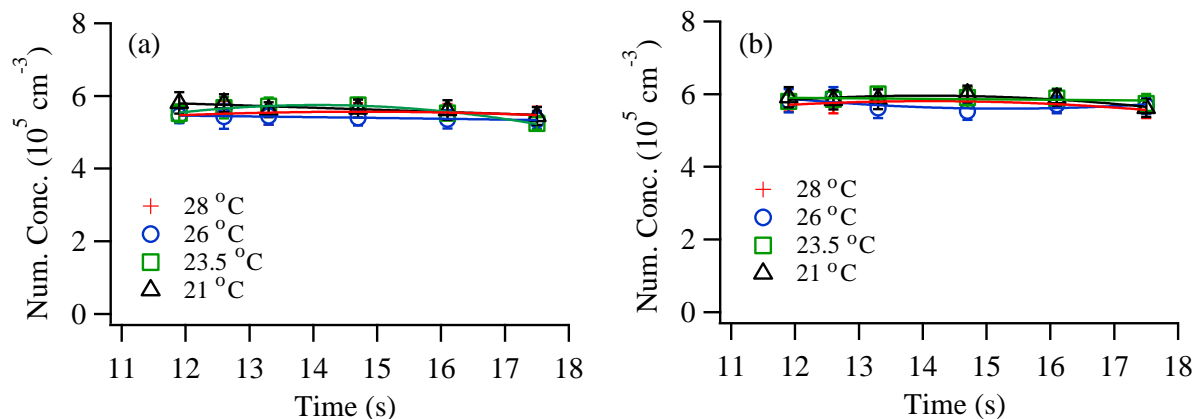56 temperature has a negligible effect on wall losses of particles over the temperature range of 21°C
57 and 28°C.

58

2

Figure S2. Number concentrations of particles as a function of time from 2.1×10^{11} cm^{-3} MSA and 2.0×10^{11} cm^{-3} MA at varied temperatures (a) under dry conditions and (b) with 2.9×10^{17} cm^{-3} H$_2$O. The lines between data points are drawn as guides to the eye. Error bars represent one standard deviation from triplicate SMPS measurements and lie within the symbols in some cases. The time on the X-axis represents the time particles travelled within the flow reactor and does not include the additional time (1.9 s) for particles to travel through the sampling tube to the SMPS.

Effects of Sampling Tube Temperature

A portion of the sampling tube outside the flow reactor was not temperature controlled. To test for possible artifacts this might cause, a control experiment was carried out by heating the portion of the sampling tube outside the flow reactor with heating tape to the same as the temperature as in the flow reactor; in this experiment, 28°C was chosen since that was the highest temperature studied here. Number concentrations and diameters of particles from the reaction of MSA and NH$_3$ collected with and without heating tape were essentially the same (Fig. S3), indicating that particle formation and growth have either fully proceeded in the flow reactor or have been quenched rapidly in the sampling tube. Thus, there is no observable artifacts from keeping the sampling tube at ambient temperature.
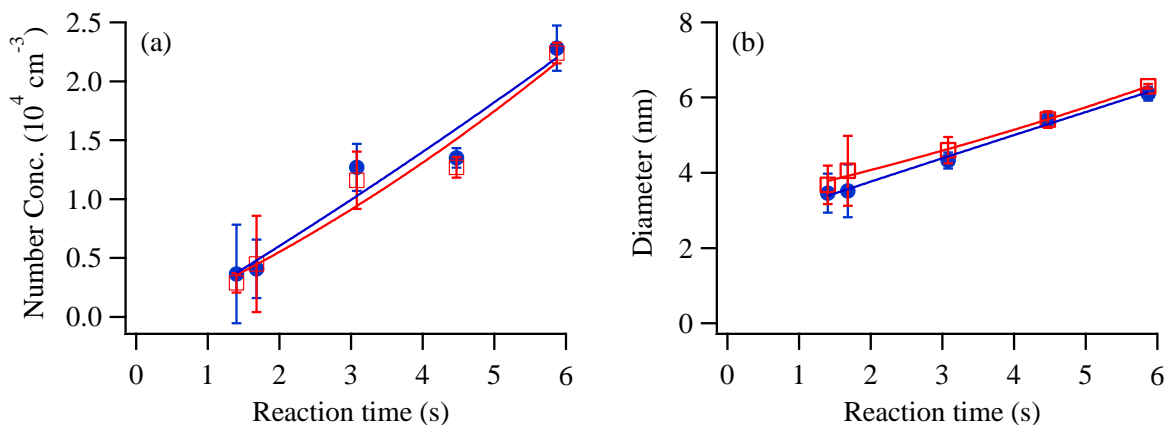
Figure S3. (a) Number concentrations and (b) diameters of particles from 2.2×10^{10} cm^{-3} MSA, 1.6×10^{11} cm^{-3} NH$_3$ and 2.9×10^{17} cm^{-3} H$_2$O at 28°C with the portion of the sampling line outside of the flow tube kept at 28°C (blue filled circles) and ambient temperature (red open squares), respectively. The lines between data points are drawn as guides to the eye. Error bars represent one standard deviation from triplicate SMPS measurements and lie within the symbols in some cases.

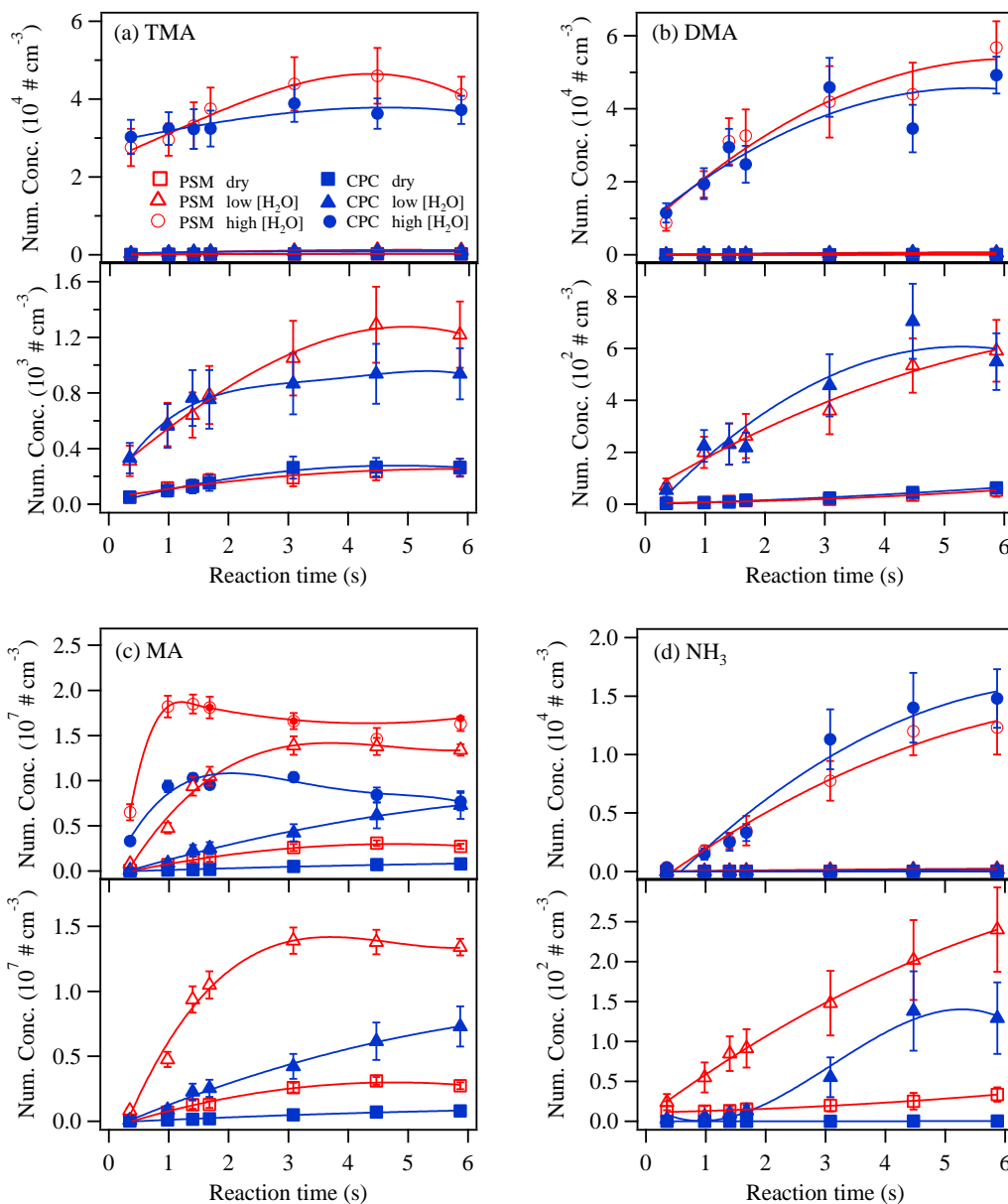**Figure S4.** Particle number concentrations measured by CPC either directly or coupled to PSM for reactions of (a) 6.4×10^{10} cm^{-3} MSA and 6.9×10^{10} cm^{-3} TMA, (b) 6.7×10^{10} cm^{-3} MSA and 6.9×10^{10} cm^{-3} DMA, (c) 6.4×10^{10} cm^{-3} MSA and 6.9×10^{10} cm^{-3} MA, and (d) 6.4×10^{10} cm^{-3} MSA and 6.9×10^{10} cm^{-3} NH$_3$ under dry conditions as well as with water vapor concentrations of $(0.5\text{-}0.6) \times 10^{17}$ cm^{-3} (low [H$_2$O]) and $(2.9\text{-}3.0) \times 10^{17}$ cm^{-3} (high [H$_2$O]) at ambient temperature (~23.5°C). The lower panel of each plot shows the expanded view of the upper one in the low number concentration region for clarity. Error bars represent one standard deviation from multiple measurements and lie within the symbols in some cases. Note that these experiments were not part of the temperature dependence studies and hence are not included in Table 1 in the main text.
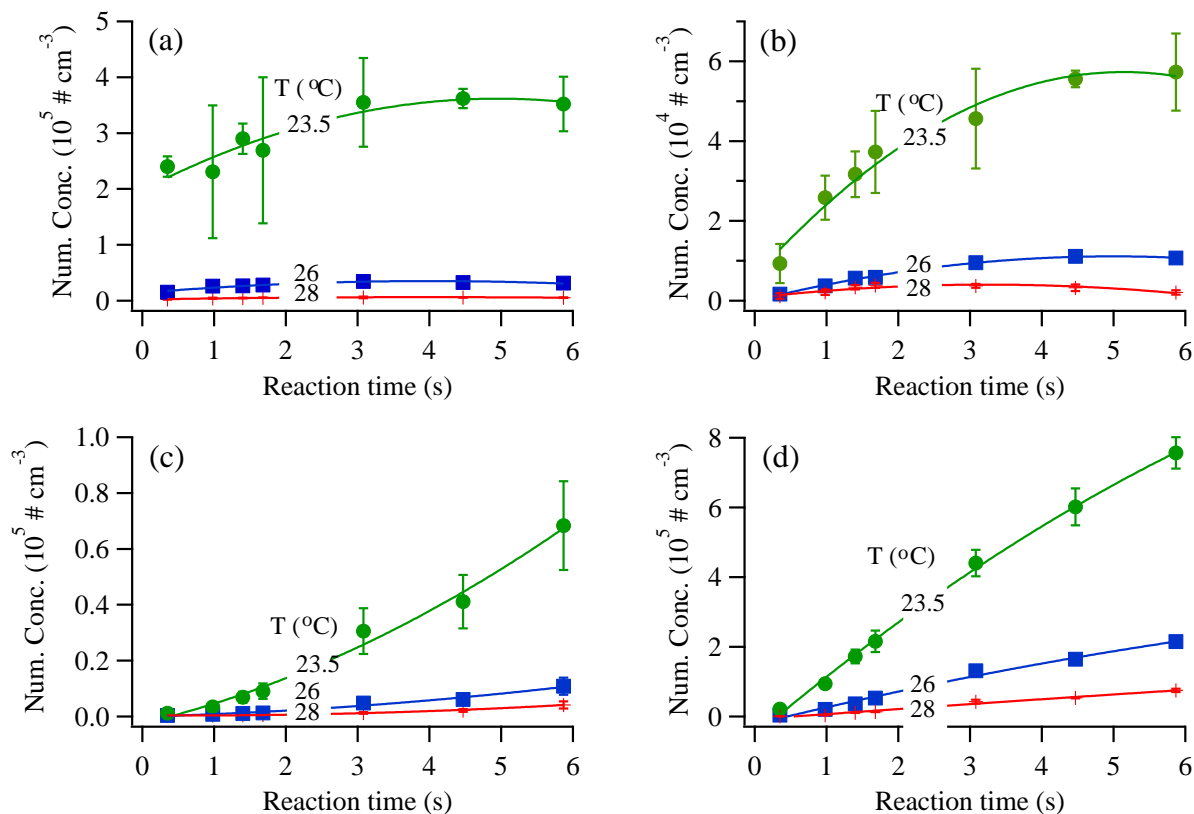
5

Figure S5. Expanded plots from Figure 1 showing number concentrations of particles as a function of time at varied temperatures from (a) 11.6×10^{10} cm^{-3} MSA, 12.8×10^{10} cm^{-3} TMA and 3.0×10^{17} cm^{-3} H$_2$O; (b) 6.7×10^{10} cm^{-3} MSA, 6.9×10^{10} cm^{-3} DMA and 2.9×10^{17} cm^{-3} H$_2$O; (c) 1.0×10^{10} cm^{-3} MSA, 2.5×10^{10} cm^{-3} MA and 2.9×10^{17} cm^{-3} H$_2$O; (d) 7.7×10^{10} cm^{-3} MSA, 21.7×10^{10} cm^{-3} NH$_3$ and 2.9×10^{17} cm^{-3} H$_2$O. The lines between data points are drawn as guides to the eye. Error bars represent one standard deviation from triplicate SMPS measurements and lie within the symbols in some cases.
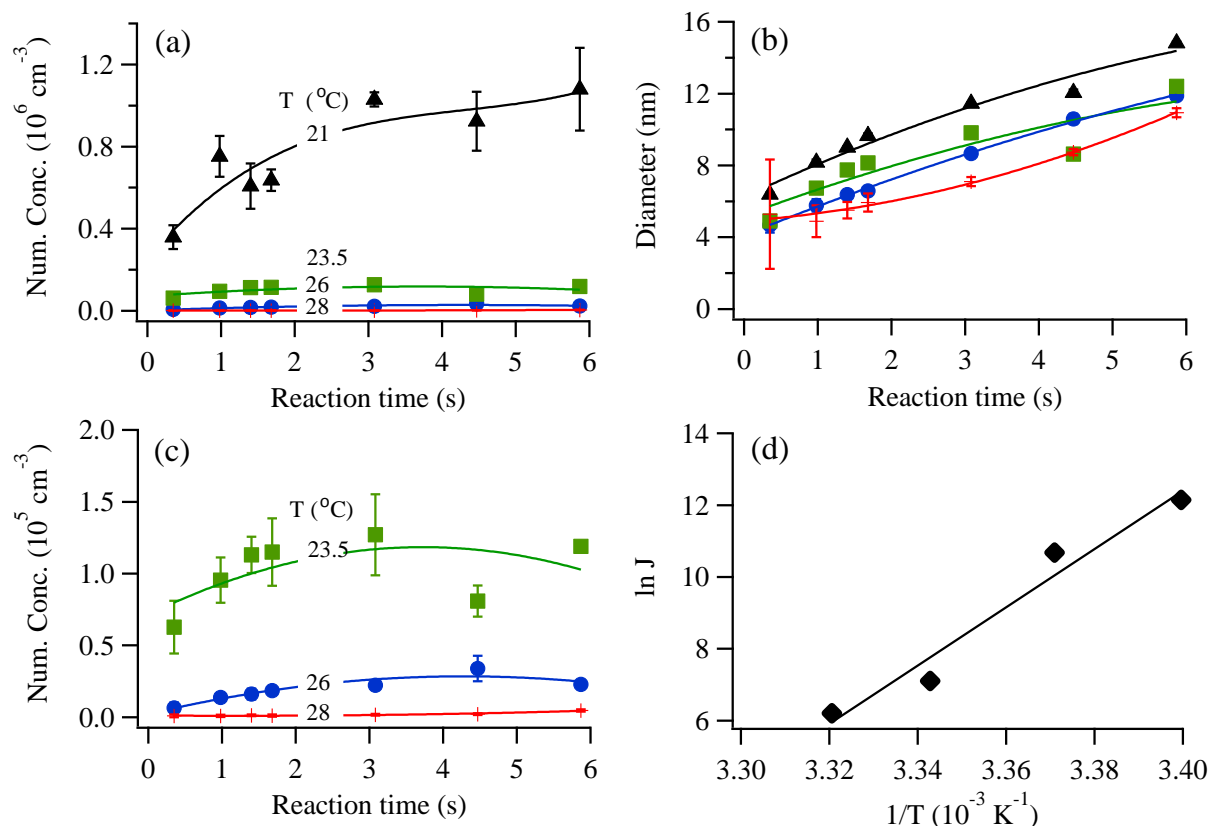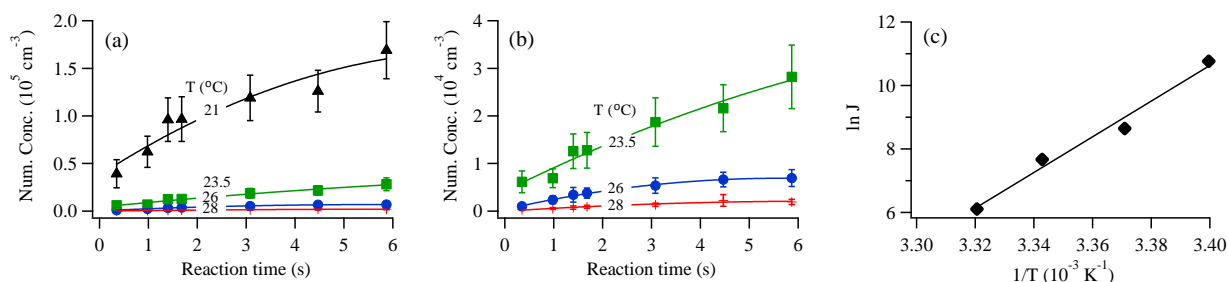
Figure S6. Typical example of (a) number concentrations and (b) diameters of particles as a function of time from 10.4×10^{10} cm^{-3} MSA and 10.4×10^{10} cm^{-3} TMA at varied temperatures under dry conditions. (c) Expanded view of (a) in the low number concentration region. The lines between data points are drawn as guides to the eye. Error bars represent one standard deviation from triplicate SMPS measurements and lie within the symbols in some cases. (d) Plot of ln *J* vs. the reciprocal absolute temperature with the corresponding linear fit. Particle formation rates *J* were calculated from (a) as described in the text.
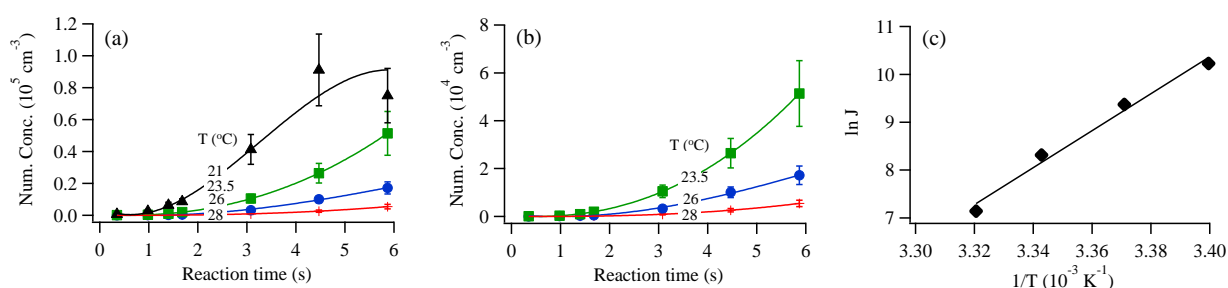
117

118

Figure S7. (a) Typical example of number concentrations of particles as a function of time from 12.8×10^{10} cm^{-3} MSA and 12.4×10^{10} cm^{-3} DMA at varied temperatures under dry conditions. (b) Expanded view of (a) in the low number concentration region. The lines between data points are drawn as guides to the eye. Error bars represent one standard deviation from multiple PSM-CPC measurements, and lie with the symbols in some cases. (c) Plot of ln J vs. the reciprocal absolute temperature with the corresponding linear fit. Particle formation rates J were calculated from (a) as described in the text.

126

127

128

129

Figure S8. (a) Typical example of number concentrations of particles as a function of time from 4.4×10^{10} cm^{-3} MSA and 3.5×10^{10} cm^{-3} MA at varied temperatures under dry conditions. (b) Expanded view of (a) in the low number concentration region. The lines between data points are drawn as guides to the eye. Error bars represent one standard deviation from multiple PSM-CPC measurements and lie within the symbols in some cases. (c) Plot of ln J vs. the reciprocal absolute temperature with the corresponding linear fit. Particle formation rates J were calculated from (a) as described in the text.
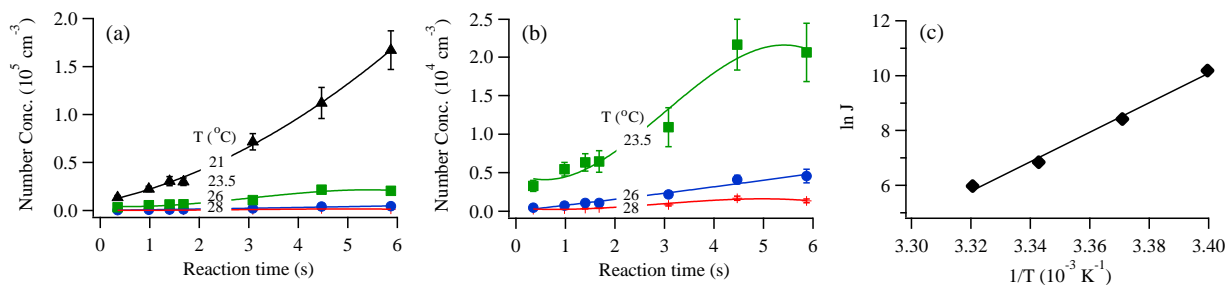
137

138
139

Figure S9. (a) Typical example of number concentrations of particles as a function of time from 9.6×10^{10} cm^{-3} MSA and 72.4×10^{10} cm^{-3} NH$_3$ at varied temperatures under dry conditions. (b) Expanded view of (a) in the low number concentration region. The lines between data points are drawn as guides to the eye. Error bars represent one standard deviation from multiple PSM-CPC measurements and lie within the symbols in some cases. (c) Plot of ln J vs. the reciprocal absolute temperature with the corresponding linear fit. Particle formation rates J were calculated from (a) as described in the text.
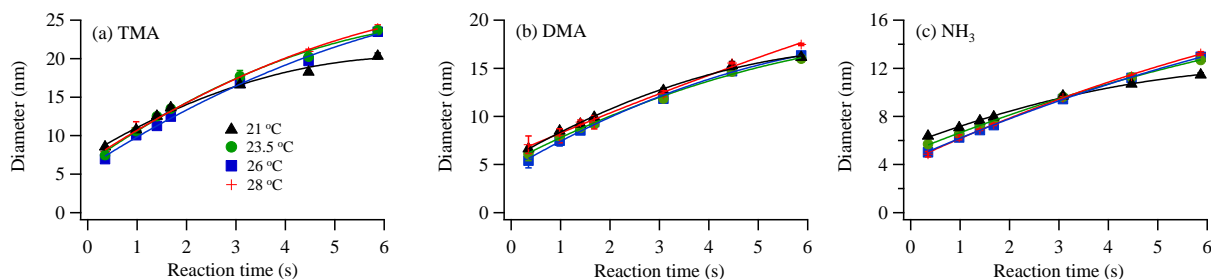
147

148

149

150

Figure S10. Typical examples of diameters of particles as a functions of time at varied temperatures from (a) 11.6×10^{10} cm^{-3} MSA, 12.8×10^{10} cm^{-3} TMA and 3.0×10^{17} cm^{-3} H$_2$O corresponding to Figure 1; (b) 6.7×10^{10} cm^{-3} MSA, 6.9×10^{10} cm^{-3} DMA and 2.9×10^{17} cm^{-3} H$_2$O corresponding to Figure 2; (c) 7.7×10^{10} cm^{-3} MSA, 21.7×10^{10} cm^{-3} NH$_3$ and 2.9×10^{17} cm^{-3} H$_2$O corresponding to Figure 4. The lines between data points are drawn as guides to the eye. Error bars represent one standard deviation from triplicate SMPS measurements and lie within the symbols in some cases.

Table S1. Diffusion coefficients in cm^2 s^{-1} for gas phase precursors at varied temperatures[a]

Temperature (°C)	21	23.5	26	28
MSA	0.099	0.101	0.103	0.104
NH$_3$	0.210	0.214	0.217	0.220
MA	0.147	0.150	0.152	0.154
DMA	0.118	0.119	0.121	0.123
TMA	0.101	0.103	0.105	0.106

[a] Diffusion coefficients estimated using the Wilke and Lee Method.[S1]

158

159

160 **References**

161 S1. C. R. Wilke and C. Y. Lee, *Ind. Eng. Chem.*, 1955, **47**, 1253-1257.